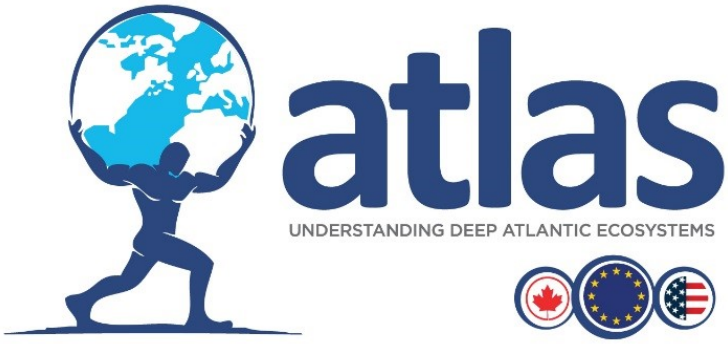

Deliverable 1.1

Lagrangian connectivity of North Atlantic ecosystems

Project acronym:	ATLAS
Grant Agreement:	678760
Deliverable number:	D1.1
Deliverable title:	Lagrangian connectivity of North Atlantic ecosystems
Work Package:	WP1
Date of completion:	
Author:	Stefan Gary, SAMS Alan Fox, HWU Arne Biastoch, GEOMAR

This project has received funding from the European Union's Horizon 2020 research and innovation programme under grant agreement No 678760 (ATLAS). This output reflects only the author's view and the European Union cannot be held responsible for any use that may be made of the information contained therein.

1 Introduction

One of the overarching goals of ATLAS is to investigate the sensitivity of North Atlantic Ocean ecosystems to the temporal variability of basin-scale physical processes. The export pathways of North Atlantic waters, embedded within temporally-varying, large-scale circulation features described by indexes such as the Subpolar Gyre Index (SPGI) and the Atlantic Meridional Overturning Circulation (AMOC), set the connectivity between ocean regions. This connectivity has impacts on the dispersal of larvae from benthic communities which are one of the primary considerations for setting the spatial domains for Marine Protected Areas.

While the time-mean circulation is generally well documented, the short observational record and strong mesoscale to interannual variability in the North Atlantic mean that the temporal variability of the circulation as well as the time-mean and temporally varying point-to-point connectivity in the North Atlantic are still open questions. Furthermore, current observational programs have made progress measuring the Eulerian variability (e.g. the SPGI [HR04] and AMOC [CKR+07][LBB+16]) but there is less certainty about the variability of Lagrangian pathways.

Here, we use output from a cutting-edge, high-resolution ocean model to estimate the envelope of variability of the Lagrangian pathways from ATLAS Case Study (CS) regions (Fig. 1) over a 50 year time scale. Since the heterogeneous, patchy nature of deep ocean ecosystems is generally at a smaller scale than the topography of even the ocean circulation model we use here, the extent of each ATLAS Case Study is viewed as an ecosystem. Our primary goals are to determine the Lagrangian pathways associated with each CS region due to just the currents and search for temporal variability in these Lagrangian pathways. Deliverable 1.5 will build on this work by exploring the impact of biological effects (e.g. pelagic larval duration and active larval swimming), which have substantial uncertainties in themselves, on the Lagrangian pathways and their variability. Our philosophy is to use the variability of the Lagrangian pathways based on just the physics as a baseline with which to interpret the impact of perturbations due to the biological parameters rather than to sort through all the possible physical and biological variability all at once.

A secondary goal is to highlight the importance of the depth off the bottom at which particles are released. Release depth can be used to account for vertical velocity gradients and vertical mixing that are unresolved in the model bottom grid boxes [BBD+16]. Furthermore, under certain conditions organisms can seed their larvae at depths that are considerably off the bottom, for example larvae entrained in plumes from hydrothermal vents or larvae preferentially released during times of stronger vertical mixing. In particular, we will test whether the pathways are sensitive to launching particles immediately at the bed or slightly higher in the water column, all released within the same bottom grid node.

ATLAS focuses on deep-sea benthic ecosystems at depths of 200 m to 2000 m, including coral reefs and gardens, sponge grounds, cold seeps and hydrothermal vents, found principally around the continental shelf break, on seamounts, offshore banks and the mid-Atlantic ridge. Our focus, most relevant to the biology being studied in ATLAS, is therefore on the pathways of the upper to intermediate depth water. These waters are also interesting from a North Atlantic variability perspective because they contribute to the upper limb of the AMOC. In Section 2 we document the Lagrangian particle tracking method used and the particle release strategy. A very brief summary of the Eulerian flow variability in the model is presented in Section 3. Then, we present the time-mean pathways from each ATLAS Case Study in Section 4. In Section 5 we document the sensitivity of the pathways to particle release depth and in Section 6 we discuss the temporal variability of the Lagrangian pathways. Finally, we summarize the results in Section 7.

2 ATLAS Case Studies and particle launch locations

The North Atlantic ATLAS Case Study regions along with particle launch locations are shown in Figure 1 and the name of each Case Study region is listed in Table 1. The ATLAS Case Study regions were chosen to coincide with important ecosystems that may be connected with each other.

Particles are simulated with the ARIANE software [BR97] based on the velocity, potential temperature, T, and salinity, S fields in the VIKING20 configuration [BBB+16] of the NEMO ocean model [Mad08]. In the VIKING20 hindcast run, forced by the CORE2 data set [LY09], a

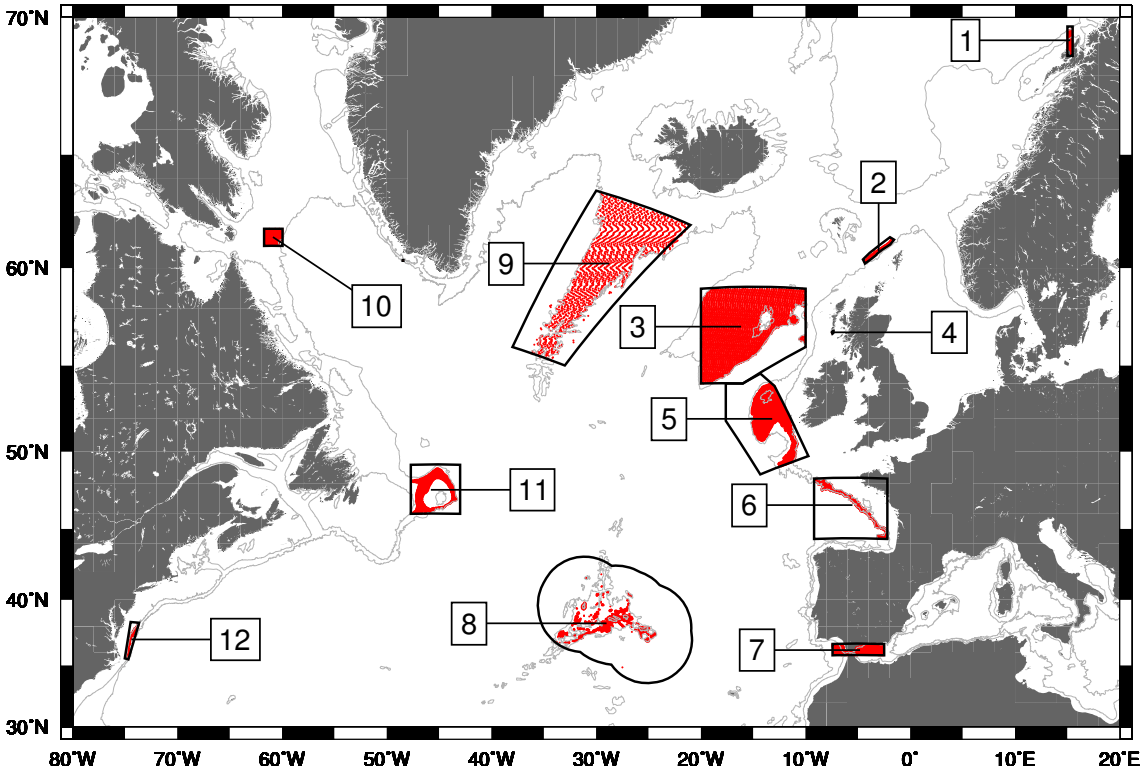

Figure 1: Map of the ATLAS Case Studies with the numbers in boxes corresponding to the left column of Table 1. Case Study polygons are shown with black lines and particle release locations are shown with red dots. The 200 m and 2000 m isobaths are shown with gray lines. Closed isobath contours with a small number of points are ommitted for clarity.

1/20°resolution grid spanning the North Atlantic was two-way nested [DVB08] within a 0.25°resolution global ocean. VIKING20 output from 1958 to 2009, at a temporal resolution of average fields over every 5 days, is used here.

The boundary for each ATLAS Case Study listed in Table 1 was set by the intersection of a polygon and a range of water depths. The VIKING20 grid nodes in the deepest boxes within a Case Study boundary were then set to be the release locations for the particles. To estimate the potential impact of unresolved vertical gradients of horizontal velocity within each bottom grid box, a particle was released near the very bottom of each box (90% of the box thickness) and near the top of each box (10% of the box thickness). Over the depth range of the particles released in this study, 30 m to 2200 m, grid boxes vary in thickness from about 10 m to 200 m. Particles were released from these bottom grid boxes at the approximate midpoint of each of the 4 seasons for each year from 1959 to 2008. The season midpoints are mid-January, mid-April, mid-July, and mid-October. We use the term "release ensemble" to refer to the group of particles that were all released together at the same time for a particular Case Study. We use the term "total ensemble" to refer to all particles released in a particular Case Study over many time steps. In all cases particle trajectories were computed for 1 year with position updates every 5 days. The "bookending" hindcast years of 1958 and 2009 allowed for computing 1-year duration trajectories backwards from the beginning of 1959 and forwards from the end of 2008, respectively, without any temporal discontinuities.

Backward trajectories were computed exactly the same as forward trajectories except that instead of stepping the velocity and tracer fields forward in time, the particles were reverse advected in the opposite direction as the currents as the velocity and tracer fields were stepped backwards in time. It is important to note here that the trajectory calculation algorithm employed in this work [BR97] advances particles along analytically calculated streamlines with no additional diffusion. In consequence, a forward trajectory from point A to point B will be identical to a backward trajectory advected from point B to point A. While forward trajectories show where particles will go if released at a specific point in space and time, backward trajectories trace the origins of particles arriving at a specific point. For the results presented here, the particles along backward

	Case Study Name	bathy min. [m]	bathy max. [m]	particles per launch	notes
1	LoVe Observatory	20	2000	1683	added points
2	Western Scottish Slope	400	600	259	
3	Rockall Bank	200	2000	4508	every 4th node
4	Mingalay Reef	100	200	729	added points
5	Porcupine Seabight	200	1200	5295	
6	Bay of Biscay	200	2000	1339	
7	Gulf of Cadiz/Alboran Sea	30	2200	1764	
8	Azores	150	1250	1968	
9	Reykjanes Ridge	200	2000	1917	every 10th node
10	Davis Strait	200	2000	950	
11	Flemish Cap	600	1450	2349	
12	US Mid-Atlantic Canyons	200	1500	302	

Table 1: Numbers of particles representing each Case Study (CS) at each release time. These numbers are the number of particles in each release ensemble. For each release time, one particle was released at every VIKING20 bottom grid node that lies within the CS polygon and the given isobath range (i.e. the red dots in Fig. 1). Particles were released at 200 discrete times: one burst of particles in the middle of each season over 50 years of the model run from 1959 to 2008. The middle of each season is defined as mid-January, mid-April, mid-July, and mid-October. Taking into account that particles were also released near the very bottom and top of each grid box, the total number of particles simulated for each CS (the total ensemble) is the number in the fifth column times 400 (400 = 50 years times 4 seasons per year times 2 launch depths). Polygons for CS01 and CS04 only encompassed a small number of model grid points, 187 and 9, respectively, so additional particles were added to the simulations by creating new particles offset by ±0.3 index units (for both) and ±0.1 index units (only for CS04) to the particles launched exactly at the grid nodes. CS03 and CS09 polygons contained too many points so the numbers of particles for those CS were cut down by subsampling the number of grid nodes at which particles were released.

trajectories (i.e. going from point B to point A) were released at exactly the same points and times as the corresponding forward trajectories (i.e. going from point B to point C) so the spreading backward in time is different from the spreading forward in time.

3 The background Eulerian variability

The basin-scale, interannual circulation of the Subpolar Gyre can be challenging to observe due to potential aliasing by the much smaller length and time scales of the vigorous eddy activity at high-latitudes. As such, several indexes have been developed to represent the flow at larger time and spatial scales.

The Subpolar Gyre Index (SPGI), as determined by an EOF decomposition of the sea surface height (SSH) field, is an indicator of the possible spin up and expansion or spin down and contraction of the Subpolar Gyre [HR04]. This index is also highly anticorrelated to sea surface height anomalies at 52°W, 57°N. The expansion (contraction) of the Subpolar Gyre is hypothesized to block (allow) warmer, saltier waters of subtropical origin from reaching the eastern subpolar North Atlantic and thus modulate large-scale changes in T and S along the eastern basin [HSD$^+$05]. The local maximum of the SPGI in the early 1990's followed by a long-term decline of the gyre circulation since the beginning of altimeter observations in 1992 to about 2010 is consistent with other multi-decadal model simulations [HLM$^+$16, BSD$^+$06] and has been shown to have a possible impact on the distribution of marine life [HLM$^+$16]. The SSH anomalies in VIKING20 (Fig. 2) are consistent with this general pattern.

Another key time series is the Atlantic Meridional Overturning Circulation (AMOC). Here, we compute the AMOC by taking the zonal integral of all meridional velocities and then finding the maximum value of the vertically integrated volume flux starting at the sea surface. Since the ATLAS Case Study sites span a wide range of latitudes, the AMOC index presented in Fig. 2 is the average of all the AMOC values obtained from about 35°N to 60°N and not at a single latitude as is usually reported. As the AMOC exhibits some meridional coherence in this latitude range

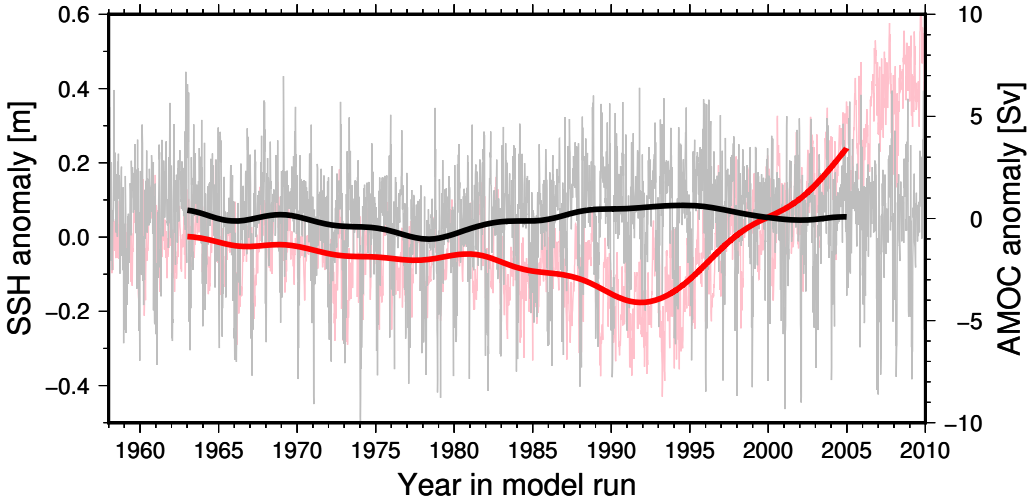

Figure 2: Red and pink lines are sea surface height (SSH) anomalies, relative to the 1958 to 2009 mean, at 52°W, 57°N in VIKING20, which is a good approximation of the Subpolar Gyre Index [HR04]. The pink line is the SSH anomalies at each 5-day average field output by the model and the thick red line is the SSH anomaly time series smoothed with a 10 year Gaussian filter. Note that positive values in this time series correspond to negative values in the SPGI and vice versa because SSH is anticorrelated with the SPGI. The gray and black lines correspond to the 5-daily and 10-year Guassian smoothed, respectively, AMOC in VIKING20 as described in the text of Section 3. The units of Sverdrups, Sv, are a volume flux of 1×10^6 m^3 s^{-1}.

[BBB+16] (see their supplementary information, Fig. 4c;a), the AMOC index in Fig. 2 is broadly similar to the AMOC at any specific latitude from about 35°N to 60°N. In the VIKING20 subpolar gyre, the AMOC is high in the 1960's, lowest in the 1970's and early 1980's, and then highest in the 1990's and early 2000's [BBB+16] (see their supplementary information, Figs. 4b;b and 4c;a and our Fig. 2). While the strongest values of the SPGI are nearly synchronous with the strongest AMOC, the decline in the SPGI in VIKING20 from the 1990's to the end of the 2000's (Fig. 2) appears to be a much bigger change than the corresponding values of the AMOC. It is important to note that the AMOC and SPGI are not necessarily consistent with each other because the SPGI is essentially a measure of the barotropic flow and neglects the subsurface baroclinic flow, an important component of the AMOC and strongest in the eastern subpolar North Atlantic [HCJ+15].

4 Overview of the particle spreading

Figures 3 through 14 show the spreading envelopes, as defined by the 95% most-likely probability contour [BBD+16] for all the particle positions of the total ensembles of each of the Case Studies. This contour is first constructed by finding the two-dimensional histograms of particle positions in x, y and T, S space at 0.25°geographic, 0.05 salinity, and 0.2 °C temperature resolutions. Then, the histogram is normalized by the total number of particle positions to create a probability map. An iterative search for the boxes with the highest probabilities that ends once 95% of all the probability is found results in mask whose outline contains 95% of the particle positions as well as the boxes with the highest probabilities. This outline is the 95% most likely particle position contour line.

The 95% most likely contours are constructed from all positions along each particle track, not just the finish positions. All points along the trajectory are used so that the pathways are displayed. Otherwise, information about the path taken to the finish point would be lost. Also, maps of contours constructed from endpoints only (or all points at just 6 months, etc.) would be more sensitive to the time span chosen than maps constructed from all the points along a trajectory.

The spreading of the forward and backward trajectories from each Case Study suggests that all the Case Studies along the boundary of the North Atlantic Basin can be part of a network of linked ecosystems via passive particle trajectories. For the most part, the Case Study links

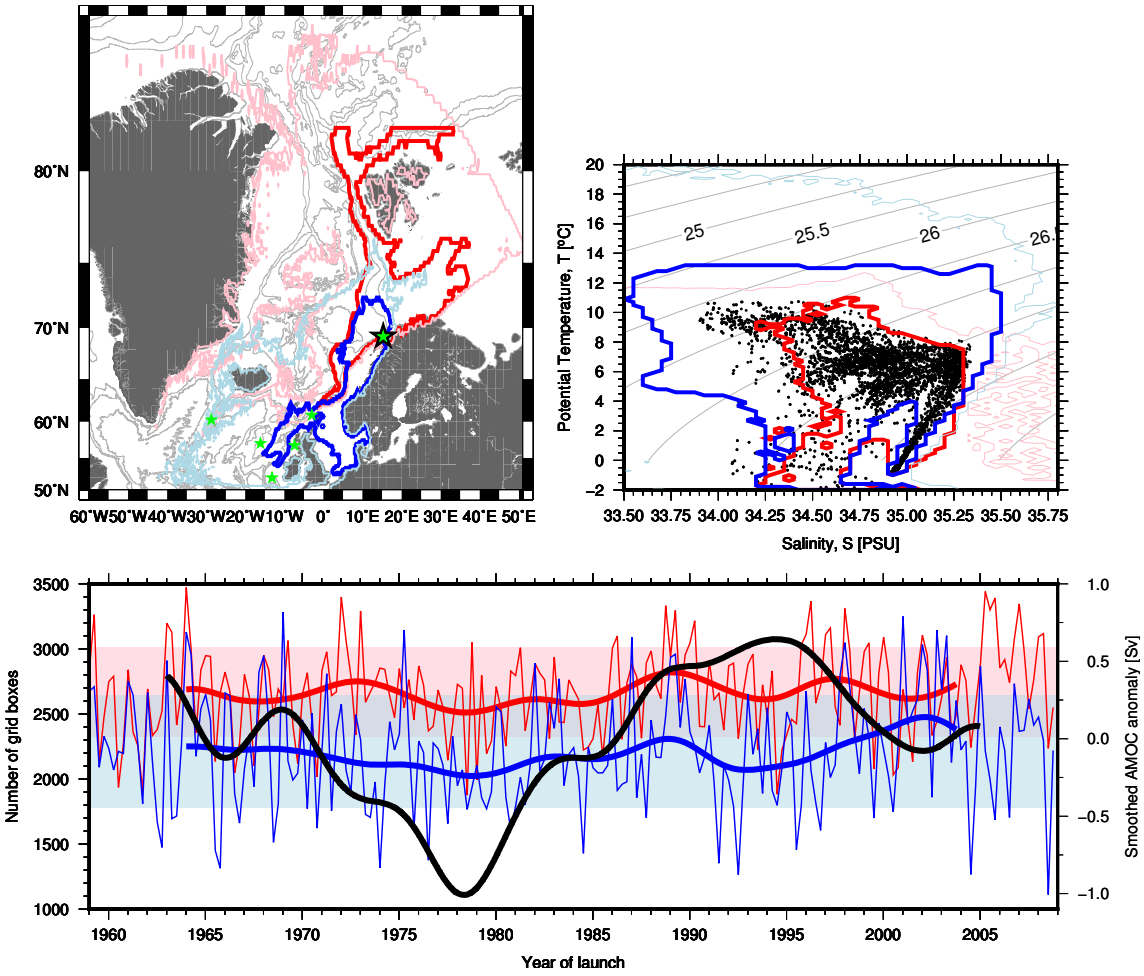

Figure 3: Map (left) and temperature salinity relationship (right) of the forward (red) and backward (blue) 95% most likely contours [BBD+16] constructed from all positions along the trajectories of all particles launched from Case Study 1. Bold lines in the top panels correspond to the 95% most likely probability contour while the lighter contours delineate the maximum extent of the spreading of all particles (i.e. 5% of the particle positions lie between the corresponding bold and light contours). For only CS01, the maximum extent of the forward spreading is constrained by the northern and eastern boundaries of the VIKING20 high resolution nest. Launch locations for Case Study 1 in x, y and T, S space are shown with the black dots (only every 100th point in T, S space). The mean locations of the case studies are shown with green stars and the star with the bold black outline is CS01. Bathymetry and isopycnals are contoured with light gray lines at 1000 m and 0.5 kg m^{-3} intervals, respectively. Time series of the extent of the 95% most likely contour line are presented in the bottom panel with red and blue lines for forward and backward trajectories, respectively. The black line is the smoothed AMOC timeseries from Fig. 2. Each point corresponds to the release ensemble started at the date given on the horizontal axis. Thick (thin) lines are smoothed with a 10 year Gaussian-weighted filter (raw data). The extent of the 95% most likely contour is defined as the number of 0.25°$\times$ 0.25°boxes that lie inside the 95% most likely contour line. At 50°N, the area of a grid box is approximately 8000 km^2. The $\pm$ 1 standard deviation polygon, relative to the mean value of each time series, is also shaded.

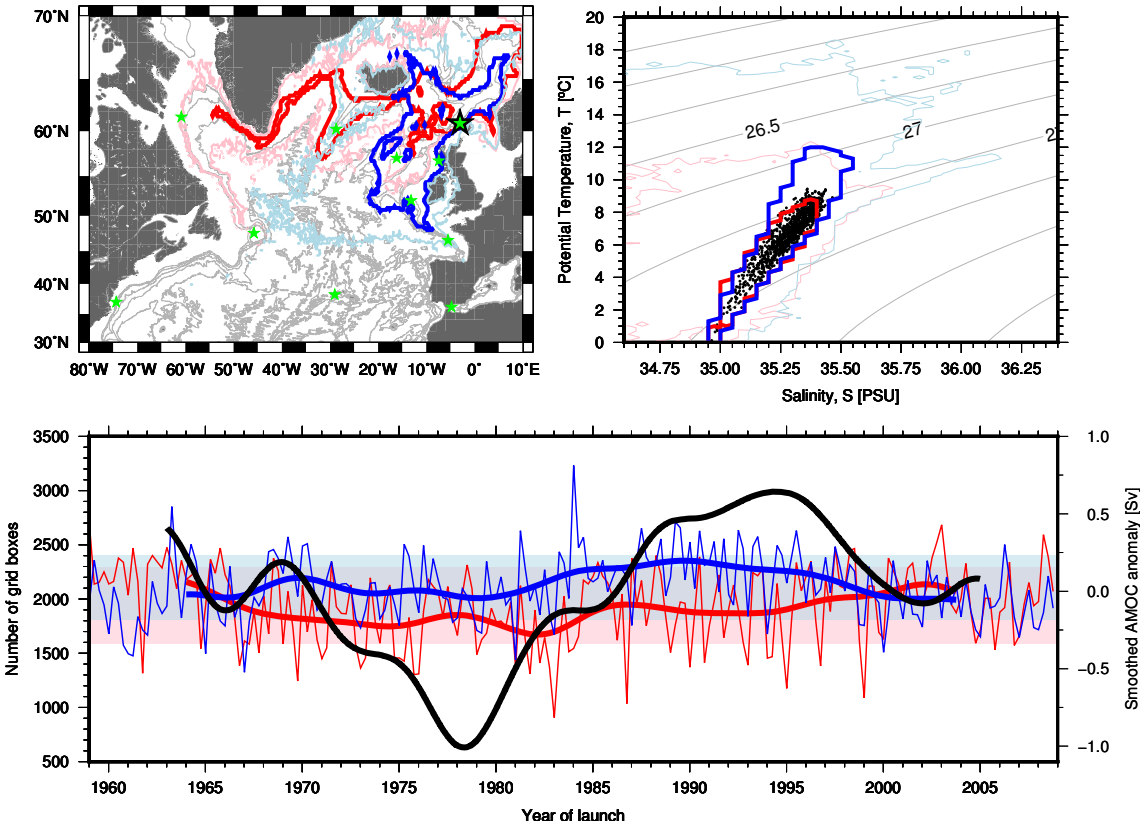

Figure 4: As in Fig. 3, but for Case Study 2.

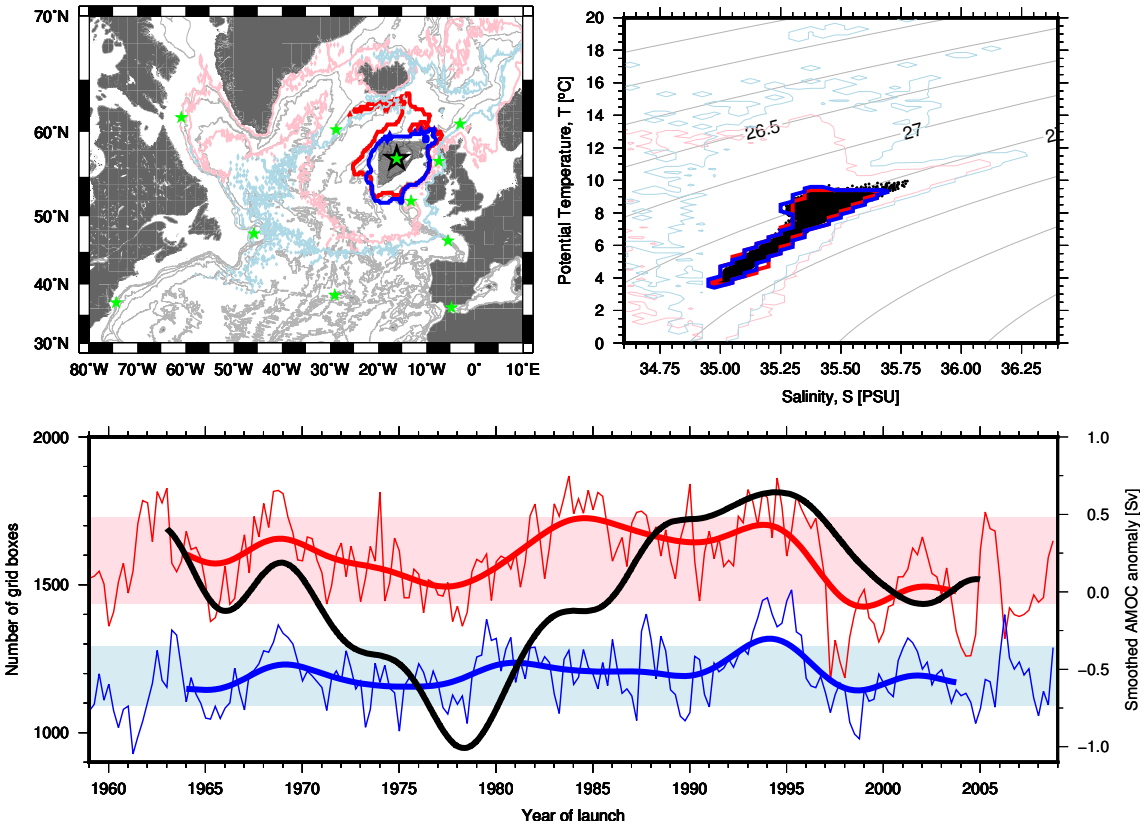

Figure 5: As in Fig. 3, but for Case Study 3.

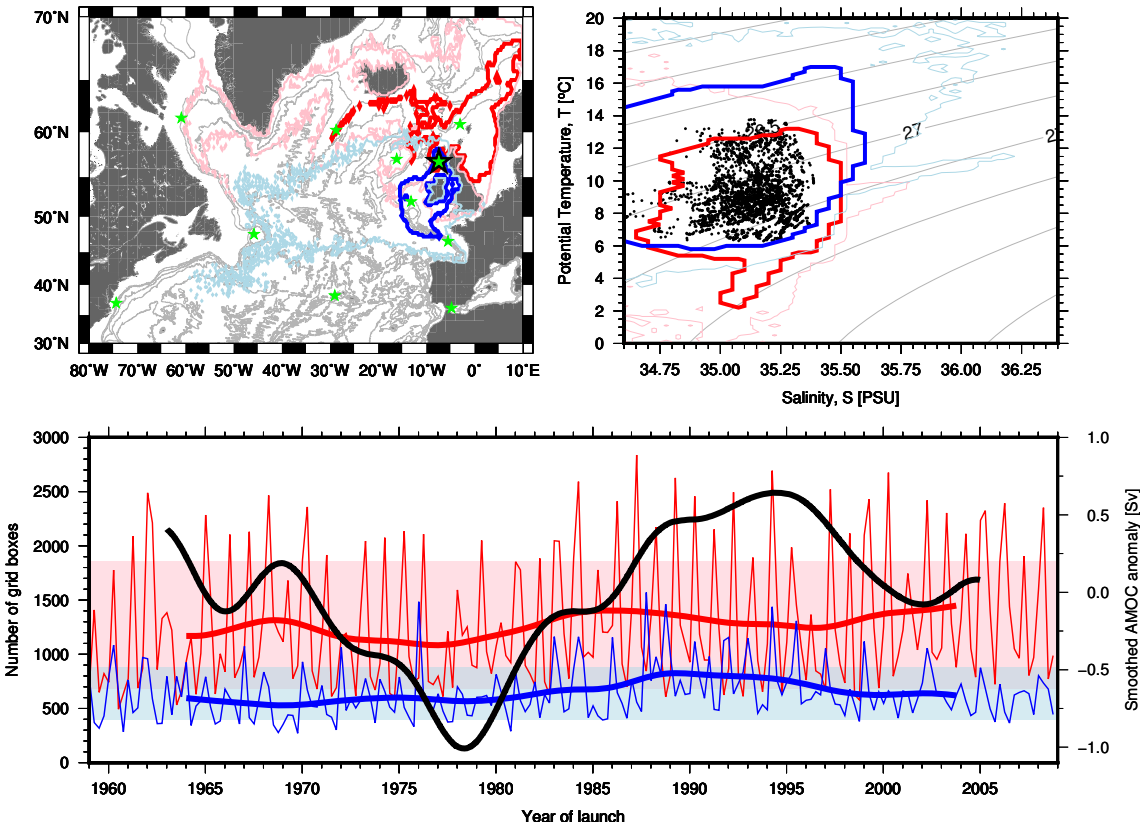

Figure 6: As in Fig. 3, but for Case Study 4. Particles experiencing very low salinities are on the continental shelf and not in the open North Atlantic.

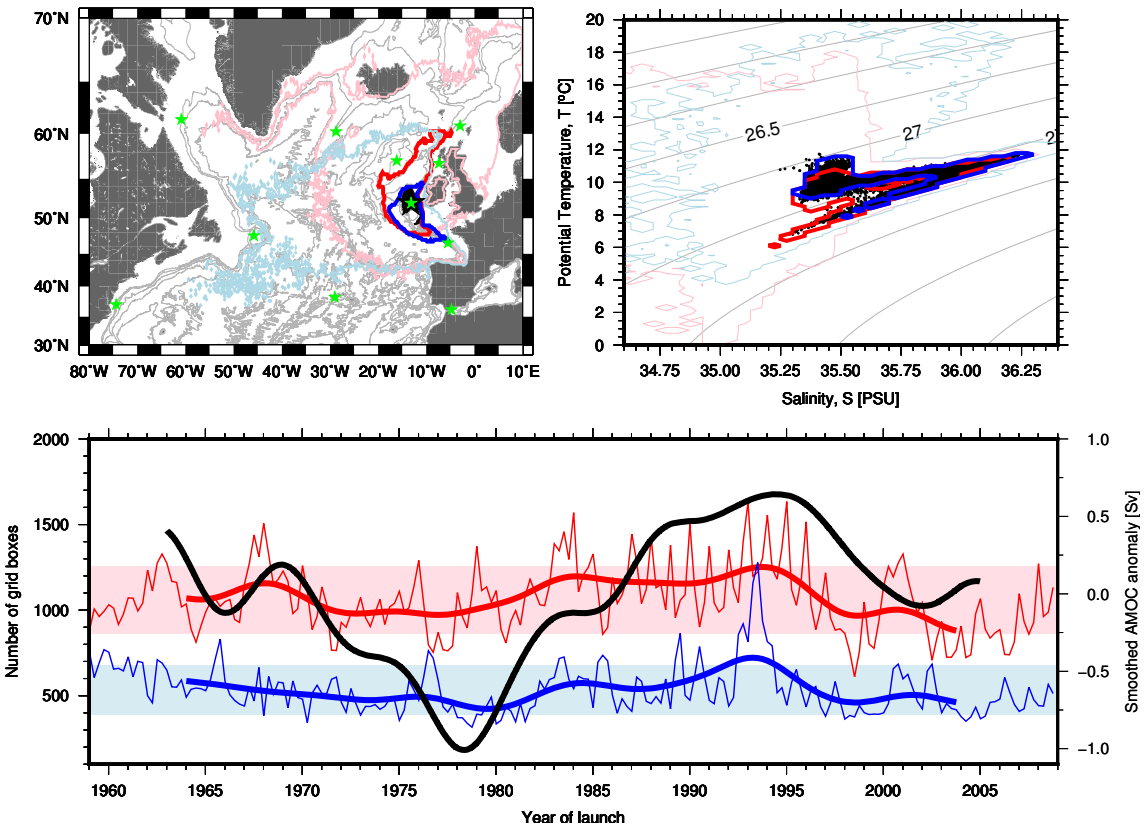

Figure 7: As in Fig. 3, but for Case Study 5.

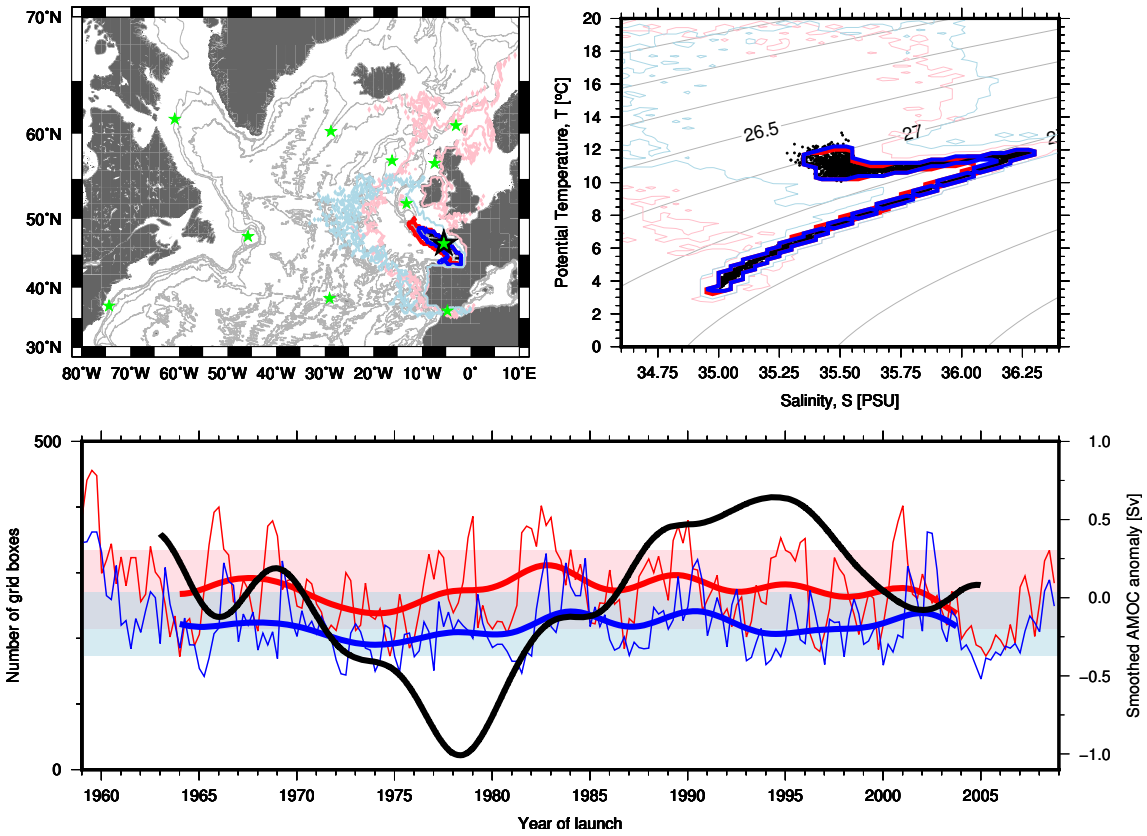

Figure 8: As in Fig. 3, but for Case Study 6.

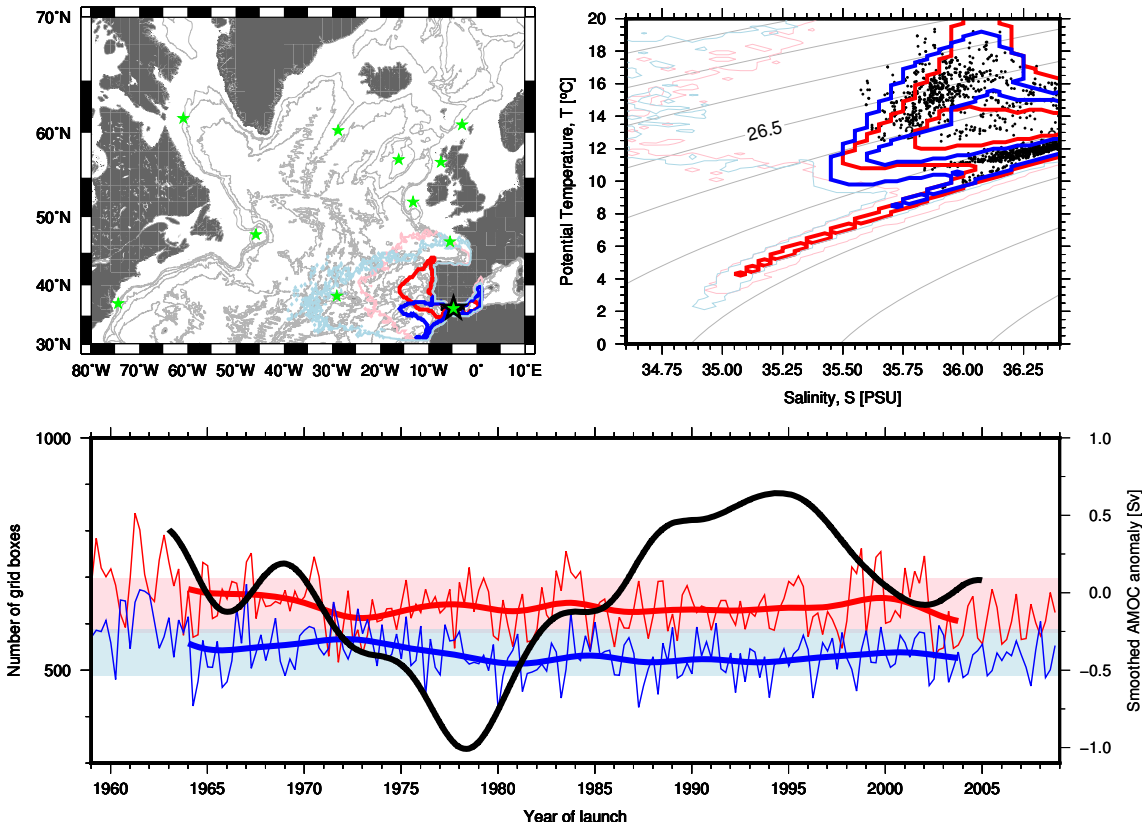

Figure 9: As in Fig. 3, but for Case Study 7. Particles experiencing very high salinities are in the Mediterranean Sea and not in the open North Atlantic.

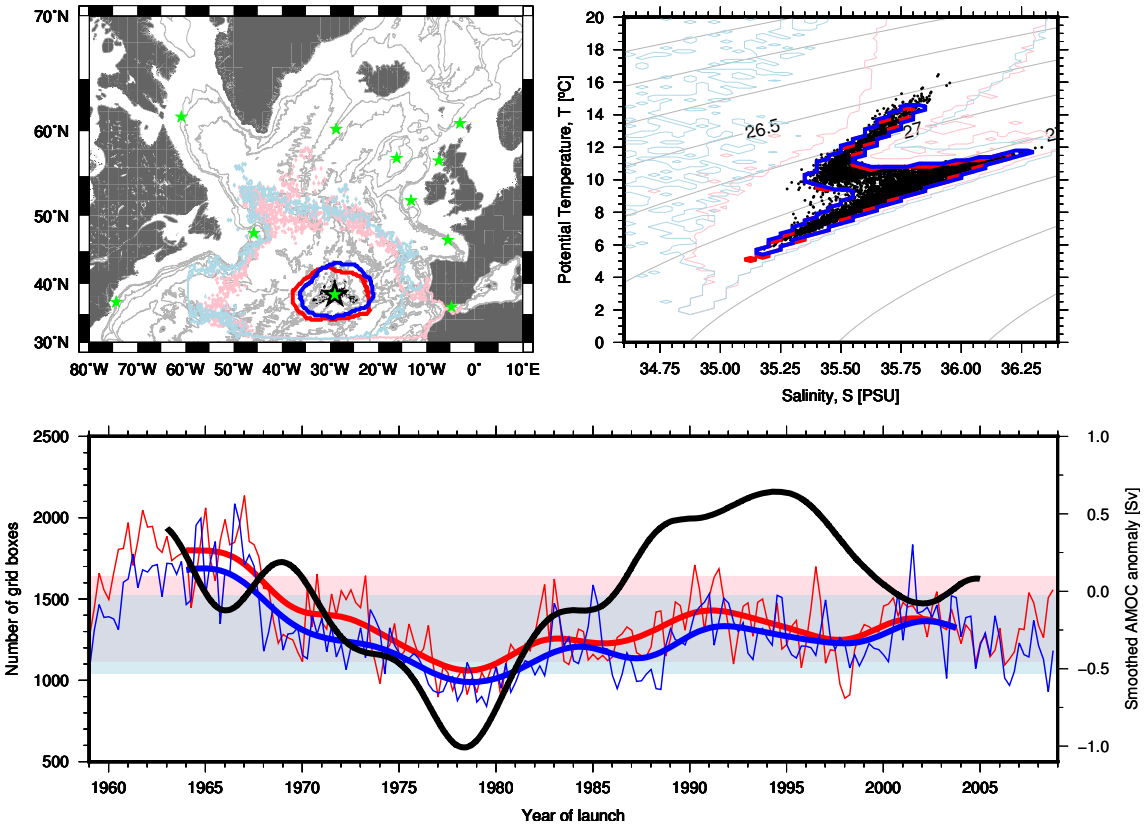

Figure 10: As in Fig. 3, but for Case Study 8.

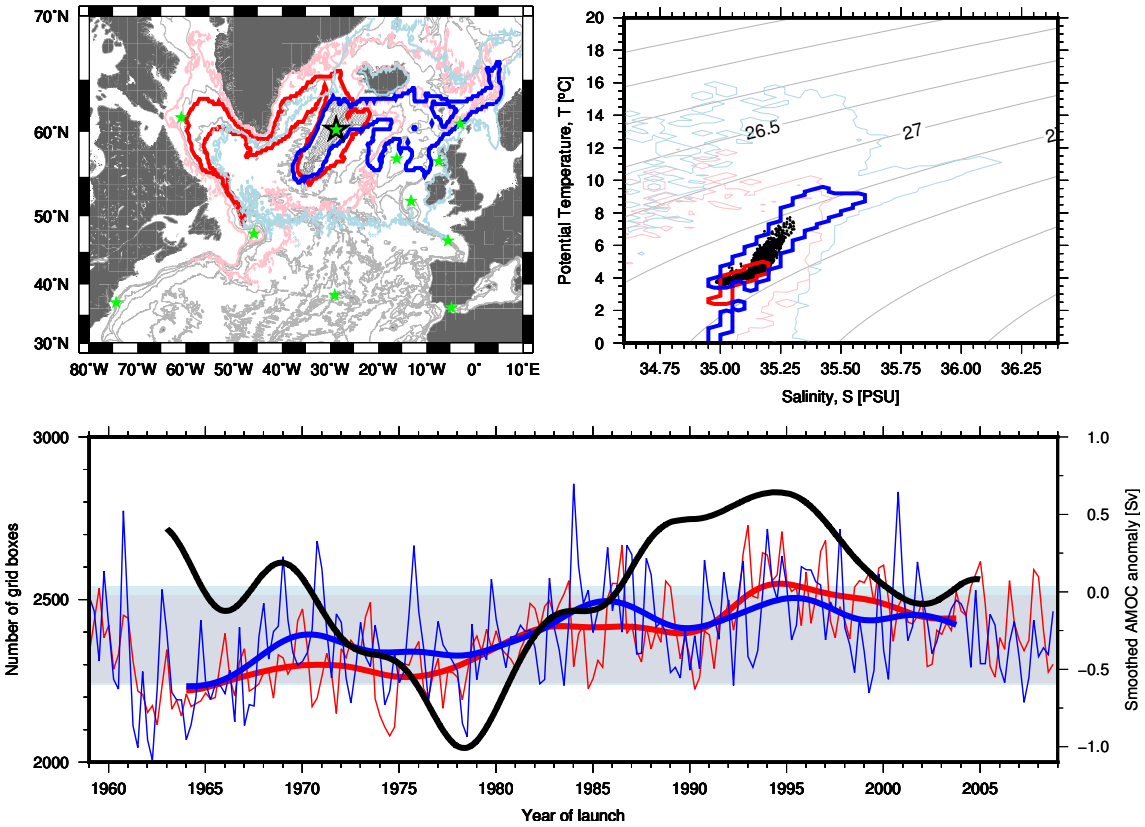

Figure 11: As in Fig. 3, but for Case Study 9.

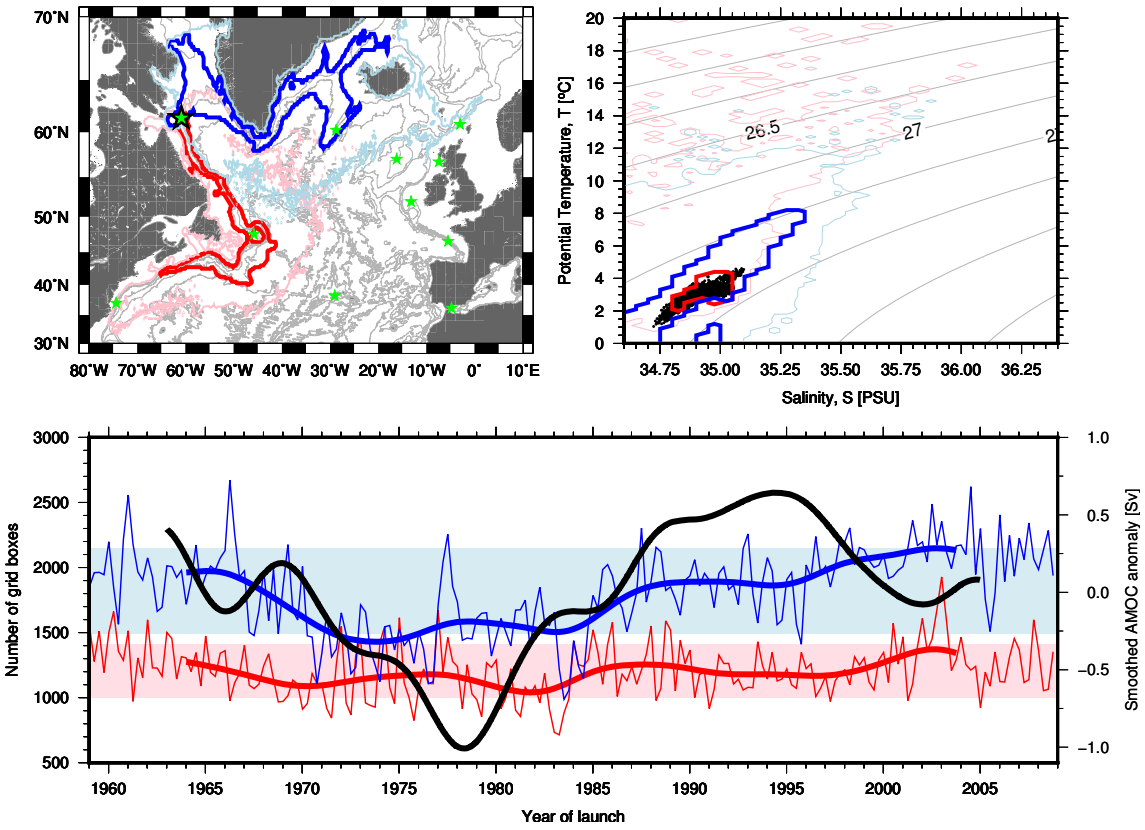

Figure 12: As in Fig. 3, but for Case Study 10. Particles experiencing very low salinities are on the continental shelf and not in the open North Atlantic.

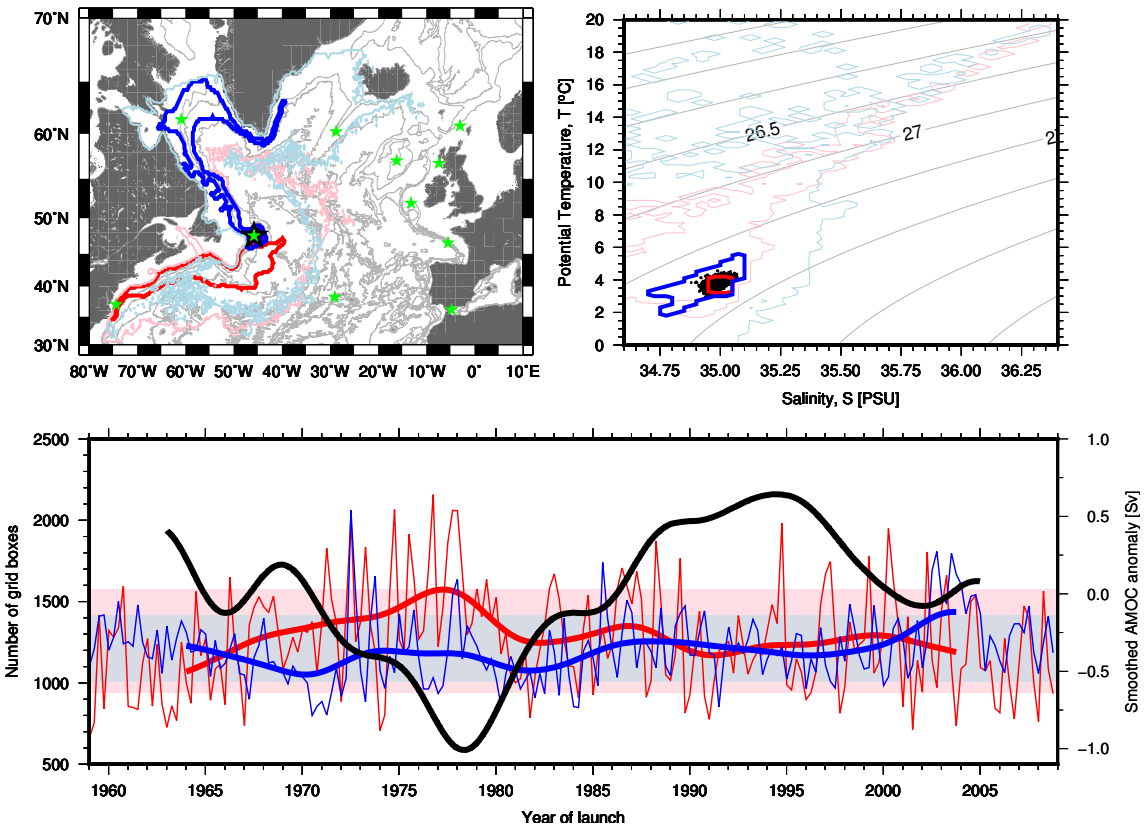

Figure 13: As in Fig. 3, but for Case Study 11.

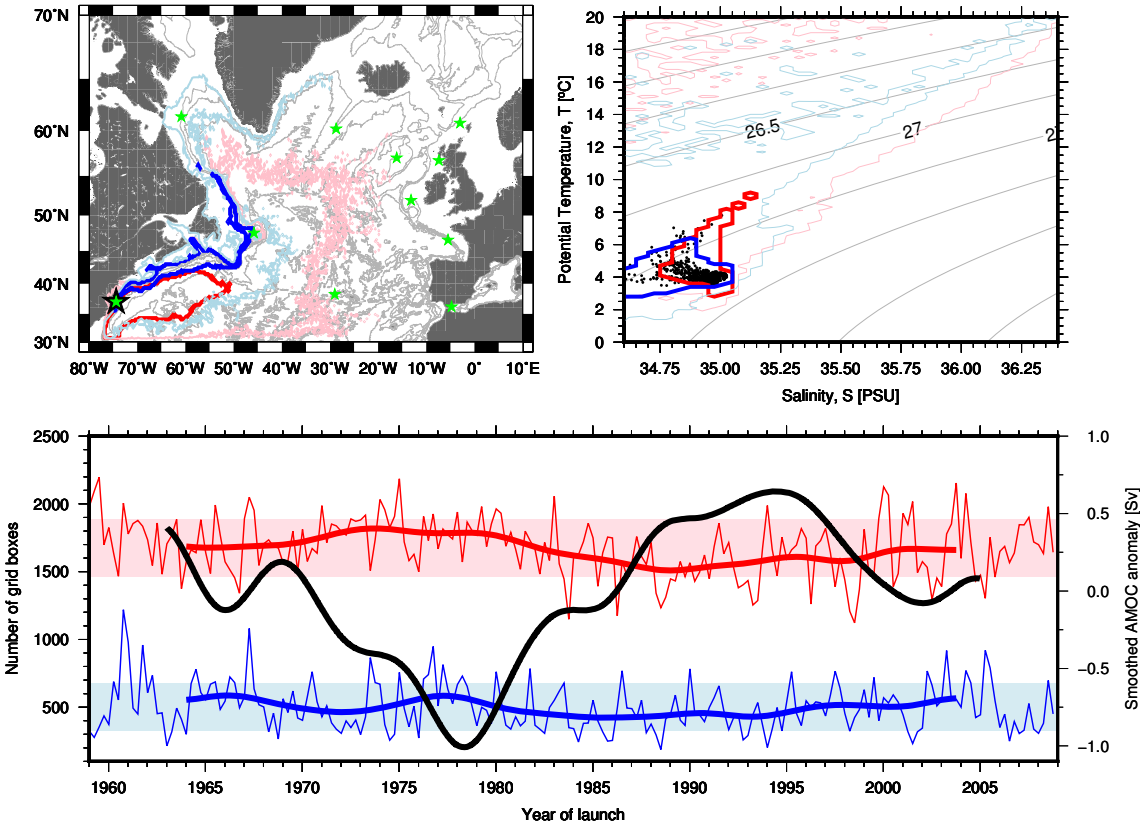

Figure 14: As in Fig. 3, but for Case Study 12. Particles experiencing very low salinities are on the continental shelf and not in the open North Atlantic.

along the basin edge are a cyclonic sequence with the order of CS08 to CS07 to CS06 to CS05 to CS03 to CS09 to CS10 to CS11 to CS12. The cyclonic rim of connectivity has a small gap in its southwestern quadrant since CS08 is just barely out of reach of CS11 and CS12. Many of the CS to CS links are at or below the 5% level (i.e. outside the 95% most likely contour but within the maximum extent of the particle spreading), highlighting the importance of "stepping stone" sites to enable population connectivity or the definition of the lateral bounds of an ecosystem.

CS01, CS02 and CS04 lie on the periphery of the main basin-edge cyclonic sequence of Case Studies. CS01, on the eastern boundary of the Nordic Seas, primarily sends particles into the open Nordic Seas or the Arctic and it can receive particles from the Northeast Atlantic, most notably CS02, CS03, and the North Sea (Fig.3). CS02, in the Faroe-Shetland Channel, receives particles from a wide range of sites (CS03, CS04, and CS05) and sends particles to CS09 (Fig. 4). CS04 lies on the continental shelf in a very different circulation regime compared to its open ocean cousins. Despite this physical isolation, CS04 is connected to a wide variety of other sites (CS06, CS05, CS03, and CS02). The dramatic change in oceanographic setting experienced by particles arriving at or leaving CS04 is shown by the large change in T, S experienced by the particles in the upper right panel of Fig. 6 compared to the primarily constant or at least isopycnal T, S changes for the other Case Studies.

5 Impact of depth of launch

For all Case Studies, no significant difference in the 95% most likely contours was detected for the particles launched near the bottom and near the top of each bottom grid node (not shown). While the spreading of particle trajectories launched at highly localized sites can be extremely sensitive to release depth and is likely a stochastic result driven by the chaotic eddy field [BBD+16], the ecosystem-wide approach taken here with particles released over many launch points means that the stochastic variability at each launch point is averaged out and the choice of launch depth is has only a minor impact. All analysis here will include both the shallow and deep released floats with equal weighting.

6 Temporal variability

While the total ensembles of trajectories from each Case Study can be used to visualize the time-mean spreading of particles from each Case Study, the temporal variability of the Lagrangian pathways to and from each Case Study is examined by repeating the spreading analysis for each of the 200 release ensembles associated with each Case Study. The extent of the 95% most likely contour for forward and backward trajectories in each release ensemble are shown in Figures 3 through 14.

Using 1-year tracks, the Lagrangian pathways show large variability on seasonal to annual timescales, much of this is due to the chaotic nature of the mesoscale eddy field. For some ATLAS Case Studies (most notably CS04) there is evidence of regular a seasonal cycle in the extent of the pathways. Examination of this is beyond the scope of this report, but will be examined in ATLAS Deliverable 1.5 in relation to variable spawning times. To examine the lower-frequency variability we smooth the data with a 10-year Gaussian-weighted filter, the resulting temporal variability of the Lagrangian pathways for the ATLAS Case Studies can be grouped into three categories: Case Studies whose Lagrangian variability is potentially related to the AMOC; Case Studies whose variability is primarily due to exchanges between the boundary currents and the interior, and Case Studies with very low variability.

CS02, CS03, CS04, CS05, and CS08 appear to have Lagrangian temporal variability that is related to the AMOC. All of these case studies exhibit relatively large extents of the 95% most likely contour in the 1960's and 1990's (times of high AMOC) and relatively small extents of the 95% most likely contour in the 1970's and early 1980's (low AMOC). In each of these Case Studies, except CS08, the backward 95% most likely contours during the 1990's reach more to the southwest than the time mean contours, the source of the increased backward extents during the 1990's in Figs. 4, 5, 6, and 7. CS03 and CS05 also exhibit forward 95% contours that expand more to the north than the time mean contours, consistent with greater forward extents during the 1990's in Figs. 5 and 7.

For CS08, both the forward and backward 95% most likely contour lines exhibit a change from large extent in the 1960's to low extent in the 1970's, then rising again in the 1990's. This variability is broadly consistent with the variability of the AMOC at this latitude in VIKING20 [BBB+16] which is lowest in the 1970's and highest in the 1990's. An anomalously low AMOC could result in more limited particle transport due to reduced advection by the large-scale currents. However, such a direct relationship between AMOC particle movement is unlikely for CS08 because the backwards and forwards 95% most likely contours generally line up with each other. If large-scale advection were playing an important role on the timescale of the trajectories presented here, the forward (backward) contour line should lie farther to the south (north) of the Case Study region consistent with the anticyclonic circulation of the Subtropical Gyre. This is not the case, either in the time-mean (Fig. 10) or for individual launch ensembles (not shown). Particles from CS08 predominantly stay within the Case Study region and any variability in Lagrangian pathways is confined to expansion and contraction of a roughly circular 95% most likely contour.

CS01, CS09, CS10, CS11, and CS12 all fall in the category of the Case Studies whose variability is dictated primarily by the interaction between the boundary current and the basin interior. Changes in the extent of the 95% most likely contours for each release ensemble for these Case Studies are mostly due to the thickness of their pathways along the basin edges rather than the length of the pathways. The thickness of the pathway indicates the extent to which the particles in the boundary current are interacting with the basin interior.

Finally, CS06 and CS07 exhibit sufficiently less temporal variability in their Lagrangian pathways than the other Case Studies to be classified as very stable in time. Both of these Case Studies lie in a relatively sheltered bay that may be less prone to the impacts of the variability of the large-scale circulation.

7 Summary

The ATLAS Case Studies, which we take here to represent key North Atlantic ecosystems, all have the potential to be linked via a sequential, cyclonic rim of connectivity spanning the Azores to the eastern Atlantic to the Mid-Atlantic Ridge to the Deep Western Boundary Current. While the Case Study to Case Study links are possible with 1 year-long particle trajectories, some of these links are not likely (i.e. the connections lie outside the 95% most likely contours). Also, the

connectivity of the Case Studies does not appear to be sensitive to the exact launch depth of the particles provided that particles are released somewhere within in the bottom grid node.

There is temporal variability in the Lagrangian pathways at each Case Study. Some of the temporal changes in the pathways appear to be a response to decadal-scale changes in the AMOC, especially for the Case Studies in the eastern subpolar North Atlantic. Other Case Studies, predominantly along the Deep Western Boundary Current (DWBC), exhibit changes in the Lagrangian pathways that are largely modulated by the exchanges between the boundary current and basin interior. Finally, two Case Studies, the Bay of Biscay and the Gulf of Cadiz, are extremely stable.

We did not find any extreme shifts in the structure of Lagrangian pathways in any of the Case Studies. We have found times when particles spread a little more or less compared to other times, but these changes are relatively small compared to the overall spreading envelopes and never involve a dramatic reorganization of the pathways. This last observation is consistent with an analogous observation from an Eulerian perspective: both the real ocean and VIKING20 exhibit the largest variability in the DWBC in the weekly to monthly time range which may obscure the longer time scale variability [FKZ+15].

All the particle trajectories used here were 1 year long; longer trajectories may be the key to identifying changes in the larger-scale circulation. However, larvae are unlikely to drift for more than a year so it may be that the temporal variability of Lagrangian pathways on biologically-relevant timescales is entirely masked by the chaotic nature of the mesoscale eddy field. Although dramatic changes of Lagrangian pathways on a biologically-relevant time scale are not immediately obvious, the physical, temporal variability in the pathways presented here provides a baseline for evaluating the impacts of the biological parameters that will be considered in Deliverable 1.5. The tremendous uncertainty in the larval biology will be a major challenge. This will be dealt with in Deliverable 1.5 by testing for how robust the spreading is over a range of larval behaviour parameters including release dates, lifespans, and vertical swimming ability.

References

[BBB+16] Claus W Böning, Erik Behrens, Arne Biastoch, Klaus Getzlaff, and Jonathan L Bamber. Emerging impact of greenland meltwater on deepwater formation in the north atlantic ocean. *Nature Geoscience*, 9:523–527, 2016.

[BBD+16] Corinna Breusing, Arne Biastoch, Annika Drews, Anna Metaxas, Didier Jollivet, Robert C Vrijenhoek, Till Bayer, Frank Melzner, Lizbeth Sayavedra, Jillian M Petersen, et al. Biophysical and population genetic models predict the presence of "phantom" stepping stones connecting mid-atlantic ridge vent ecosystems. *Current Biology*, 26(17):2257–2267, 2016.

[BR97] Bruno Blanke and Stéphane Raynaud. Kinematics of the pacific equatorial undercurrent: An eulerian and lagrangian approach from gcm results. *Journal of Physical Oceanography*, 27(6):1038–1053, 1997.

[BSD+06] Claus W Böning, Markus Scheinert, Joachim Dengg, Arne Biastoch, and Andreas Funk. Decadal variability of subpolar gyre transport and its reverberation in the north atlantic overturning. *Geophysical Research Letters*, 33(21), 2006.

[CKR+07] Stuart A Cunningham, Torsten Kanzow, Darren Rayner, Molly O Baringer, William E Johns, Jochem Marotzke, Hannah R Longworth, Elizabeth M Grant, Joël J-M Hirschi, Lisa M Beal, et al. Temporal variability of the atlantic meridional overturning circulation at 26.5 n. *science*, 317(5840):935–938, 2007.

[DVB08] Laurent Debreu, Christophe Vouland, and Eric Blayo. Agrif: Adaptive grid refinement in fortran. *Computers & Geosciences*, 34(1):8–13, 2008.

[FKZ+15] Jürgen Fischer, Johannes Karstensen, Rainer Zantopp, Martin Visbeck, Arne Biastoch, Erik Behrens, Claus W Böning, Detlef Quadfasel, Kerstin Jochumsen, Hedinn Valdimarsson, et al. Intra-seasonal variability of the dwbc in the western subpolar north atlantic. *Progress in Oceanography*, 132:233–249, 2015.

[HCJ+15] NP Holliday, SA Cunningham, C Johnson, SF Gary, C Griffiths, JF Read, and T Sherwin. Multidecadal variability of potential temperature, salinity, and transport in the eastern subpolar north atlantic. *Journal of Geophysical Research: Oceans*, 120(9):5945–5967, 2015.

[HLM+16] H Hátún, Katja Lohmann, Daniela Matei, Johann H Jungclaus, S Pacariz, M Bersch, A Gislason, J Ólafsson, and PC Reid. An inflated subpolar gyre blows life toward the northeastern atlantic. *Progress in Oceanography*, 147:49–66, 2016.

[HR04] Sirpa Häkkinen and Peter B Rhines. Decline of subpolar north atlantic circulation during the 1990s. *Science*, 304(5670):555–559, 2004.

[HSD+05] Hjálmar Hátún, Anne Britt Sandø, Helge Drange, Bogi Hansen, and Heðinn Valdimarsson. Influence of the atlantic subpolar gyre on the thermohaline circulation. *Science*, 309(5742):1841–1844, 2005.

[LBB+16] M Susan Lozier, Sheldon Bacon, Amy S Bower, Stuart A Cunningham, M Femke de Jong, Laura de Steur, Brad deYoung, Jürgen Fischer, Stefan F Gary, Blair JW Greenan, et al. Overturning in the subpolar north atlantic program: a new international ocean observing system. *Bulletin of the American Meteorological Society*, (2016), 2016.

[LY09] WG Large and SG Yeager. The global climatology of an interannually varying air–sea flux data set. *Climate Dynamics*, 33(2-3):341–364, 2009.

[Mad08] G Madec. Nemo ocean general circulation model reference manuel. In *Internal Report*. LODYC/IPSL Paris, 2008.

Document Information

EU Project N°	678760	**Acronym**	ATLAS
Full Title	A trans-Atlantic assessment and deep-water ecosystem-based spatial management plan for Europe		
Project website	www.eu-atlas.org		

Deliverable	**N°**	D1.1	**Title**	Lagrangian connectivity of North Atlantic ecosystems
Work Package	**N°**	WP1	**Title**	Ocean Dynamics Driving Ecosystem Response

Date of delivery	**Contractual**		**Actual**	
Dissemination level				

Authors (Partner)	**SAMS**			
Responsible Authors	**Name**	Stefan Gary	**Email**	Stefan.Gary@sams.ac.uk

Version log			
Issue Date	**Revision N°**	**Author**	**Change**